Photometric Redshift Determination with the BATC Multicolor System

LIFANG XIA, XU ZHOU, JUN MA, HONG WU, WEI-HSIN SUN, ZHAOJI JIANG, SUIJIAN XUE,
JIANSHENG CHEN, AND WENPING CHEN

National Astronomical Observatories, Chinese Academy of Sciences, Beijing 100012, People's Republic of China; xlf@vega.bac.pku.edu.cn

ABSTRACT. In this paper, we present the methodology of photometric redshift determination with the BATC 15 color system by using the *hyperz* program. Both simulated galaxies and real galaxies with known redshifts were used to estimate the accuracy of redshifts inferred from multicolor photometry. From the test with simulated galaxies, the uncertainty in the inferred redshifts is about 0.02–0.03 for a given range of photometric uncertainty of 0.05–0.10 mag. The results with the 27 real galaxies are in good agreement with the simulated ones. The advantage of using the BATC intermediate-band system to derive redshift is clear after comparison with the *UBVRI* broadband system. The accuracy in redshift determination with the BATC system is mainly affected by the selection of filters and the photometric uncertainties in the observation. When we take the limiting magnitudes of the 15 filters into account, we find that redshift can be determined with good accuracy for galaxies with redshifts less than 0.5, using only filters with central wavelengths shorter than 6000 Å.

1. INTRODUCTION

In multicolor photometric surveys, the redshifts of a large number of objects in a given field can readily be obtained from the color information. Although multicolor photometry does not yield redshift information as accurately as spectroscopy does, it has the virtues of deeper limiting magnitude, faster batch reduction, and better time saving from the simultaneous determination of redshifts of many objects in a given field. With the redshifts determined for a large sample of galaxies via multicolor photometry, astronomers are able to study statistically the evolution of galaxies in number as well as in luminosity (Pascarelle, Lanzetta, & Fernández-Soto 1998; Volonteri et al. 2000; Gal et al. 2000). In a simulation using 40 bands, the efficiency of photometric redshift determination for faint objects is comparable to slitless spectroscopy (Hickson, Gibson, & Callaghan 1994). The techniques of photometric redshift are thus said to be not only the "poor person's redshift machine" but also the only viable way so far to acquire redshift information for a large quantity of faint objects, because the majority of these objects will still remain beyond the limit of spectroscopy in the foreseeable future (Bolzonella, Miralles, & Pelló 2000).

A number of computer codes performing photometry fitting have been developed and applied to data acquired in several survey projects, such as HDF, SDSS, CADIS, etc. (Sowards et al. 1999; Yahata et al. 2000; Wolf et al. 2001). Two methods have been widely used: one is the "empirical training set" method (Connolly et al. 1995; Wang, Bahcall, & Turner 1998), and the other is the "spectral energy distribution" (SED) fitting method.

The empirical training set method determines redshifts by the empirical linear relation between magnitudes (or colors) and redshifts. Although this method requires no assumptions on galaxy spectra and their evolution, there are still a few shortages. For example, the empirical relation changes with the data obtained with different filter sets. Furthermore, in high redshifts, the sample of spectroscopic templates becomes smaller and less complete, which makes redshift determination less reliable. The SED fitting method, on the other hand, is based on the fit of the overall shape of a spectrum; i.e., it relies on the detection of apparent spectral properties such as Lyman forest and Balmer jump, etc. The fitting is performed by comparing the observed SEDs to the template spectra acquired using the same photometric system (Corbin et al. 2000; Fontana et al. 2000).

The Beijing-Arizona-Taipei-Connecticut (BATC) large-field sky survey in 15 intermediate-band colors commenced in 1994. Over the years, the survey has produced a database that can be used to derive the redshifts of nearby galaxies between $z = 0$ and 0.5, providing essential information regarding the structure of the local universe and nearby galaxy clusters, especially Abell clusters (Yuan et al. 2001). The purpose of the study in this paper is to estimate the accuracy of z_{phot} using the BATC 15 color photometric system.

The organization of this paper is as follows. In § 2, we describe the BATC photometric system and the observations of two fields used as the real sample. The procedures of data reduction are discussed briefly in § 3. The application of the z_{phot} code *hyperz* is described in § 4. In § 5, a comparison between the BATC system and the *UBVRI* system using the simulation test is shown, along with the filter dependence of
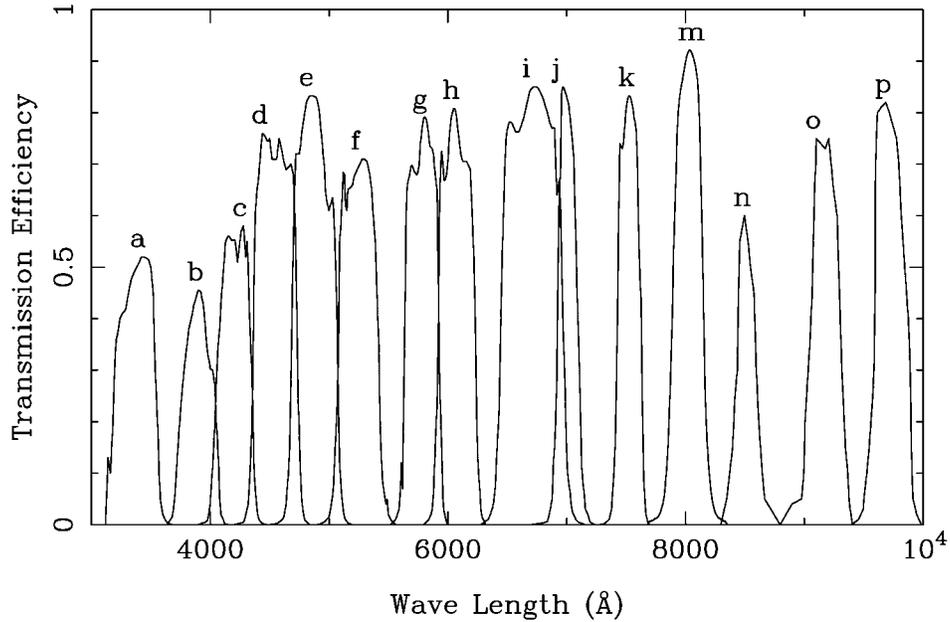
Fig. 1.—Transmission curves of the 15 BATC filters. Labels are given on top of each transmission curve.

z_{phot}. We compare the results of z_{phot} with the spectroscopic redshifts z_{spec} in § 6. Discussions and conclusions are presented in § 7.

2. THE BATC PHOTOMETRIC SYSTEM AND OBSERVATIONS

The BATC sky survey performs photometric observations with a large-field multicolor system. The observations are carried out with the 60/90 cm f/3 Schmidt Telescope of the Na-

TABLE 1
CENTRAL WAVELENGTHS AND EFFECTIVE
BANDPASSES OF THE 15 BATC FILTERS

Number	Filter	Wavelength (Å)	Bandpass (Å)
1	a	3372.1	337.85
2	b	3895.3	266.65
3	c	4202.4	282.07
4	d	4547.4	355.53
5	e	4873.3	347.12
6	f	5248.4	331.49
7	g	5784.7	271.67
8	h	6074.3	289.77
9	i	6710.8	497.00
10	j	7011.3	170.62
11	k	7527.5	191.91
12	m	8025.4	260.27
13	n	8518.2	185.40
14	o	9173.8	269.48
15	p	9724.7	278.20

tional Astronomical Observatories, Chinese Academy of Sciences (NAOC), located at the Xinglong station. A Ford Aerospace 2048 × 2048 CCD camera with 15 μm pixel size is mounted at the main focus of the Schmidt telescope. The field of view is 58 × 58 arcmin^2 with a plate scale of 1".7 pixel^{-1}.

There are 15 intermediate-band filters in the BATC filter system, which covers an optical wavelength range from 3000 to 10000 Å (Fan et al. 1996; Zhou et al. 2001). The filters are specifically designed to avoid contamination from most of the strong and variable night-sky emission lines. The filter transmission curves are shown in Figure 1, and the corresponding parameters are tabulated in Table 1.

As in the definition of the AB$_\nu$ system of Oke & Gunn (1983), the magnitudes of the BATC system is defined as follows:

$$m_{\text{BATC}} = -2.5 \log \tilde{F}_\nu - 48.60, \tag{1}$$

where $\tilde{F}_\nu$ is the flux per unit frequency in units of ergs s^{-1} cm^{-2} Hz^{-1} (Fan et al. 1996; Yan et al. 2000). The advantage of the AB$_\nu$ system is that the magnitude is directly related to the physical units. The four Oke & Gunn (1983) standards are used for flux calibration in the BATC survey. These four stars are BD +17°4708, BD +26°2606, HD 84937, and HD 19445. The magnitudes of these standards were refined by several authors. Fukugita et al. (1996) presented the latest recalibrated fluxes of these four standards. Their magnitudes have also been corrected with the BATC photometric system (Zhou et al. 2001).

When performing flat-field correction for our large-format

CCD, a simple method was applied to reach very high quality in flat-fielding. This high quality in flat-fielding is achieved by placing an isotropic diffuser in front of the Schmidt correction plate and illuminating the diffuser with scattered light from the dome screen. Normally 12 dome flat-field images are taken in each filter band within 24 hr of observation.

There are two target fields in the survey for the comparison between z_{phot} and z_{spec}: the BATC TA03 field and the BATC T329 field. The TA03 field is centered on the galaxy cluster Abell 566 with redshifts around 0.1. The spectroscopic redshifts of the 10 central galaxies in this field are given by Slinglend et al. (1998). The T329 field is centered on a high-redshift quasar, located at $\alpha = 9^h56^m25\overset{s}{.}2$, $\delta = +47°34'42\overset{''}{.}0$ with $z = 4.457$. The redshifts of 17 galaxies in this field are presented by Postman et al. (1996) and Holden et al. (1999). These information can be found in NASA/IPAC Extragalactic Database (NED).[1] The redshift information of the total of 27 galaxies from these two fields is used to check the quality of the BATC z_{phot}.

3. DATA REDUCTION PROCEDURES

The BATC survey images are reduced through standard procedures, including bias subtraction, flat-field correction, and coordinate and flux calibrations (see Fan et al. 1996; Zhou et al. 2001, 2002 for details).

After the basic corrections described above, the flat-field images and the field images observed in the same filter in the same night are combined, respectively. During combination, bad pixels and cosmic rays are removed. The *Hubble Space Telescope* (*HST*) Guide Star Catalog (GSC; Jenkner et al. 1990) is then used for coordinate determination. The final rms error in coincidence with the GSC stars is about 0″.5. The BATC photometry code was developed based on Stetson's DAOPHOT procedures (Stetson 1987). Magnitudes derived via the point-spread function (PSF) fitting method as well as the aperture photometry method are given for every source detected in the fields. The limiting magnitude in general is about 20 mag with an error of about 0.1 mag in all bands.

PSF fitting is used basically to obtain an estimate of magnitude for a point source. Our PSF magnitudes were obtained through an automatic data reduction code, PIPELINE I, developed as a standard procedure in the BATC multicolor sky survey (Fan et al. 1996; Zhou et al. 2001). A distant galaxy that is small in angular size can be regarded as a point source. Although the PSF fitting magnitude is different from the total integrated magnitude, the shape of the SED of a galaxy should not change much. Furthermore, for crowded fields, aperture photometry may not lead to results as accurate as PSF fitting codes. So PSF photometry provides another approach in addition to the aperture photometry. It will be scientifically in-

teresting to compare the accuracy in redshift determination using these two methods. We have thus carried out the estimate of photometric redshift using the magnitudes derived in each filter via both PSF fitting and aperture photometry.

For larger galaxies showing obviously extended morphology, their magnitudes obtained via PSF fitting would have larger uncertainties than for smaller galaxies. In this case, the aperture photometry method should be adopted.

Most galaxies in the T329 field are faint and small in angular size, in which case the PSF fitting method is suitable to use. For comparison, we use both PSF fitting magnitudes and aperture magnitudes to estimate redshifts of these galaxies. The results and discussions are given in § 6. The 10 galaxies in the center of the other field, Abell 566, are the brightest ones in this galaxy cluster and show obviously extended structure in the images. We thus use only magnitudes from aperture photometry. The radius of aperture adopted is 5 pixels, which corresponds to a sky projection of 8″.5.

4. SED FITTING METHOD

The SED fitting method is to fit the spectrum of an object that should include several strong spectral features such as 4000 Å break, Lyman-forest decrement, etc. We use the *hyperz* program developed by Bolzonella et al. (2000) to estimate the redshifts of galaxies. The standard χ^2 minimization, i.e., computing and minimizing the deviations between photometric SED of an object and the template SEDs obtained with the same photometric system, is used in the fitting process. The minimum χ^2 indicates the best fit to the observed SED by the set of template spectra:

$$\chi^2(z) = \sum_{i=1}^{N_{filt}} \left[\frac{F_{obs,i} - bF_{temp,i}(z)}{\sigma_i} \right]^2, \qquad (2)$$

where $F_{obs,i}$, $F_{temp,i}$, and σ_i are the observed fluxes, template fluxes, and the photometric uncertainty in filter i, respectively; b is the normalization constant, while N_{filt} is the number of filters used in the observations.

In the *hyperz* program, a number of spectra templates can be used, including the enlarged galaxy evolutionary library of Bruzual & Charlot (1993), as well as the empirical template. The parameters involved in the template construction contain star formation rate type, initial mass function, metallicity, and age of stellar population, etc. Synthetic template that has been used the most is the GISSEL 98 template (Bruzual & Charlot 1993). On the other hand, the empirical template generally used is obtained through the averaged spectra of observed local field galaxies (Coleman, Wu, & Weedman 1980) and is suitable only for low-redshift galaxies. The validity of direct extension to high-redshift objects using this template still needs to be tested. It has been shown that the synthetic and empirical templates give almost the same accuracy for z_{phot} (Massarotti, Iovino, &

---

[1] http://nedwww.ipac.caltech.edu.

Buzzoni 2001a). In this work, we used the GISSEL 98 template for redshift determination.

Fluxes given by synthetic SED models need further corrections for the interstellar medium (ISM) and intergalactic medium (IGM) extinction effects. There are different reddening laws for ISM extinction corrections. In this paper, the reddening law of Allen (1976) for the Milky Way is adopted. The IGM, on the other hand, affects dramatically the ionizing continuum blueward of redshifted Lyα, which makes the Lyman forest the most important spectral feature for objects with redshifts beyond 2.0. However, as a result of the survey depth of the BATC images, almost all the objects observed have redshifts less than 0.5, for which the Lyman forest has a minimal effect and does not enter into the wavelength range of concern and thus has no effect on our analysis. We thus do not take into account the extinction effect of the IGM.

The most obvious and useful spectral feature in redshift determination with the BATC system is then the 4000 Å Balmer break, which falls in the redshifted wavelength range of approximately 4000–6000 Å, corresponding to the BATC filters from b to h. The observations made with filters whose central wavelengths are shorter than 6000 Å are therefore extremely crucial for the success of this project. We will reinforce this point in § 5.

5. SIMULATION TEST OF BATC PHOTOMETRIC REDSHIFT

5.1. Comparison between BATC and *UBVRI* Filter Systems

In the *hyperz* program, the procedure *makecatalog* checks the self-consistency of the SED fitting method for a given photometric system. To examine the dependence of z_{phot} uncertainty on photometric errors, we use this program to build a catalog containing simulated galaxies of different redshifts and types. Gaussian distribution of magnitude error in different filters is assumed. To compare the BATC filter system to the *UBVRI* filter system of the Canada-France-Hawaii Telescope (CFHT), we created a catalog of 1000 galaxies using the total of 20 filters (15 BATC and five *UBVRI* filters) simultaneously. It is thus guaranteed that the comparison between the two systems is done for the same sample with the same redshifts. The redshift range in the simulation is set to be $z = 0$–6; z_{phot} of the 1000 galaxies are then estimated using the BATC system and *UBVRI* system, respectively. Photometric uncertainties of 0.03, 0.05, 0.1, 0.2, and 0.3 mag are assumed. To maximize the efficiency of computing when fitting, we choose the increment in redshift to be $z_{\text{step}} = 0.05$, and $Av_{\text{step}} = 0.2$ in an Av range of 0–1.2 following the values given by Bolzonella et al. (2000).

Figure 2 shows the results of photometric and catalog redshifts (z_{phot} vs. z_{cat}) with uncertainties of 0.05, 0.10, and 0.20 mag, respectively. The quality of the z_{phot} estimation with the two systems is summarized in Table 2.

The quality of z_{phot} estimation with simulated photometric errors is evaluated using the following parameters: l, $\overline{\Delta z}$, and σ_z.

The first one, l, is the catastrophic percentage of the determination, which is the ratio of incorrect determinations over the total number of estimations:

$$l = \frac{N_{\text{incrt}}}{N_{\text{total}}}, \tag{3}$$

where N_{incrt} is the number obtained using the following formula:

$$\frac{1}{\text{threshold}} < \frac{1 + z_{\text{phot}}}{1 + z_{\text{spec}}} < \text{threshold}; \tag{4}$$

here the threshold is taken to be 1.25, which means that the difference between the estimated SED and the original SED is greater than -0.20 and less than 0.25 at a given wavelength. The systematic error $\overline{\Delta z}$ is defined as the mean difference $\overline{\Delta z} = \sum \Delta z / N_g$. The standard deviation of the estimation excluding the catastrophic identifications σ_z is given by

$$\sigma_z^2 = \sum_{i=1}^{N_g} \frac{(\Delta z - \overline{\Delta z})^2}{N_g - 1}, \tag{5}$$

where N_g is the number of galaxies excluding l.

We first discuss the results of estimation of z_{phot} using the BATC system. From Table 2, we can see that, for the smallest photometric uncertainty $\Delta m = 0.03$ mag, we obtain the best fit with $\sigma_z = 0.019$ and $l = 0$, which means that all 1000 galaxies are estimated correctly. The choice of the small photometric errors anywhere between 0.03 and 0.05 does not affect the results significantly. With the increase of photometric uncertainties from $\Delta m = 0.05$ to 0.1 mag, σ_z and l also increase, i.e., from $\sigma_z = 0.021$ and $l = 0$ to 0.042 and 0.4%. Figure 2 shows this trend: especially when $\Delta m = 0.2$ mag, the scatter becomes significantly larger. The increasing scatter for $\Delta m = 0.2$ mag is caused by the ambiguity in the spectra created with large photometric uncertainty, which leads to confusion when the program tries to identify certain features. Therefore, as long as the accuracy of our photometry meets the criterion, reasonable redshift estimation is guaranteed.

With Table 2 and Figure 2, we see the distinct advantage of the BATC photometric system over the *UBVRI* system. For $\Delta m = 0.05$ mag, the performance is $\sigma_z = 0.021$, $l = 0\%$ for the BATC system and $\sigma_z = 0.174$, $l = 6.7\%$ for the *UBVRI* system. At this level of uncertainty, a large number of galaxies have already dropped out of the acceptable region for the *UBVRI* system. On the other hand, the deviation is very small with the BATC system at this level of uncertainty, and all estimates are within the acceptable range.

Figure 2 also shows large dispersion and persistent scatter even for the smallest photometric uncertainty using the *UBVRI*
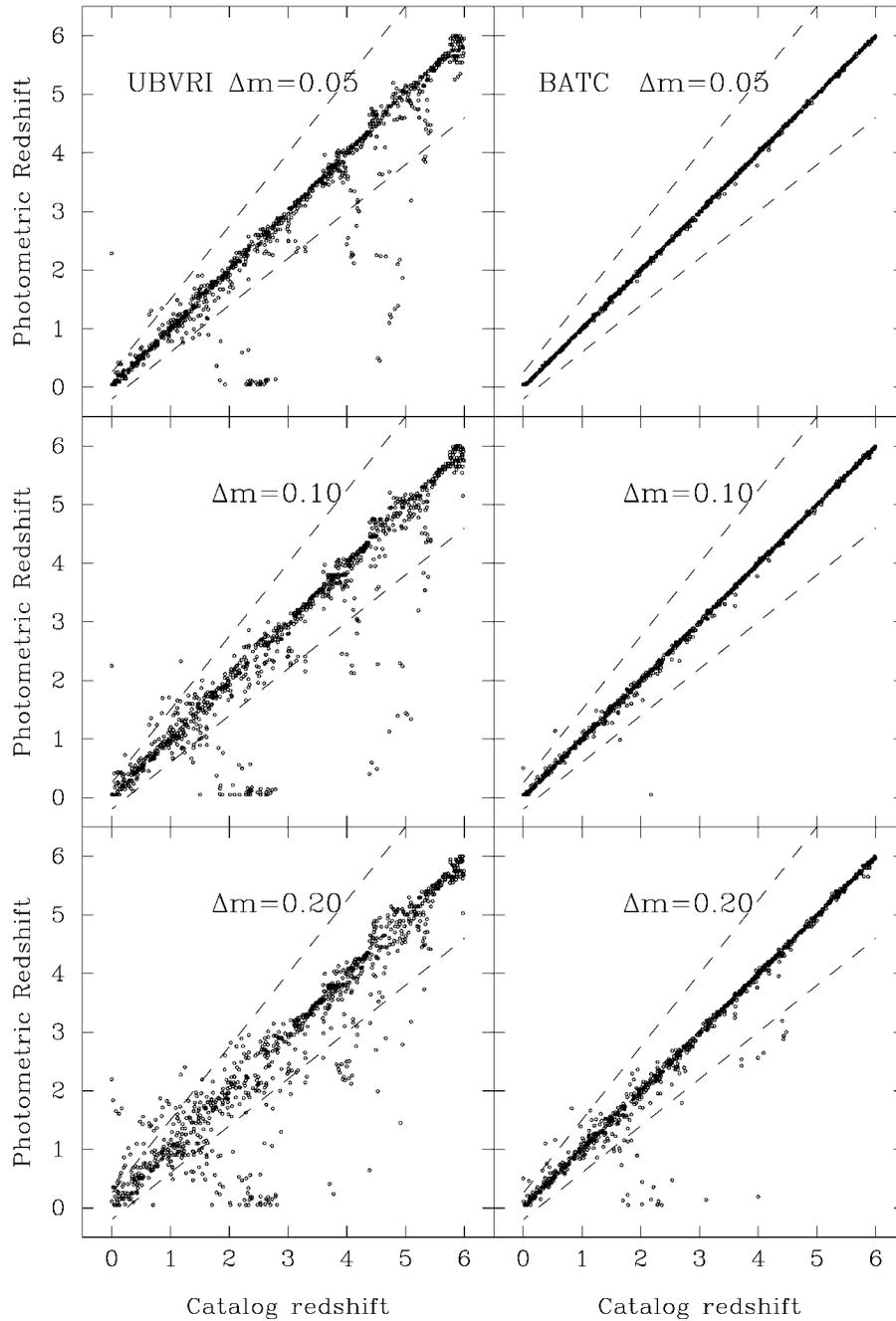
FIG. 2.—Plot of the catalog redshifts vs. the fitted redshifts (z_{cat} vs. z_{phot}) with the BATC system and the *UBVRI* system with photometric errors of 0.5, 0.1, and 0.2 mag, respectively. Redshift range is from $z = 0$ to 6. Dashed lines separate the catastrophic failures from the reasonable fits. The circles located between the two dashed lines are regarded as good estimations.

system. This is due to the smaller number and larger bandwidth of the filters, which makes the system less sensitive to delicate spectral features. For example, in the redshift range between 2.0 and 3.0, the *UBVRI* system is less sensitive to the difference between the redshifted Lyman forest and the rest-frame Balmer break.

From Table 2, we can also see that the performance of the BATC system with even the largest observational uncertainty $\Delta m = 0.2$ mag is still better than the *UBVRI* system with the smallest uncertainty $\Delta m = 0.03$ mag.

A number of studies have used *UBVRI* system for redshift determination. These studies with broadband filters give a gen-

TABLE 2
COMPARISON OF z_{PHOT} BETWEEN THE TWO SYSTEMS

	σ_z		l		$\overline{\Delta z}$	
Δm	BATC	*UBVRI*	BATC	*UBVRI*	BATC	*UBVRI*
0.03	0.019	0.163	0.0	4.3	−0.003	−0.037
0.05	0.021	0.174	0.0	6.7	−0.003	−0.043
0.10	0.042	0.195	0.4	8.9	−0.007	−0.046
0.20	0.084	0.234	3.8	13.8	−0.014	−0.056
0.30	0.133	0.324	8.0	20.7	−0.029	−0.050

NOTE.—σ_z is the dispersion excluding those catastrophic failures, l is the percentage of galaxies with redshift errors greater than 0.25 in $1 + z$, and $\overline{\Delta z}$ is the mean difference excluding l. Redshift range is from 0 to 6.

eral accuracy of around $\sigma_z \sim 0.15$ (Fontana et al. 2000; Massarotti et al. 2001a, 2001b; Le Borgne & Rocca-Volmerange 2002). The relevant studies and results are summarized in Table 3.

The study in this paper shows that the accuracy of redshift determination with the BATC system can reach 0.02–0.03 with Δm from 0.05 to 0.1 mag. This conclusion is in good agreement with that from Hickson et al. (1994), who has performed a computer simulation for a multinarrowband system of 40 bands to investigate the potential of determining galaxy morphological type and redshift. The results in their study show that, for a signal-to-noise ratio of 10, σ_z is less than 0.02; for a signal-to-noise ratio of 3, σ_z is 0.06 with redshift $z < 0.5$ and about 0.03 with $0.5 < z < 1.0$. Thus, the accuracy of our simulated photometric redshift with the BATC 15 color system agrees very well with Hickson et al. (1994).

However, the limiting magnitude of the BATC system is about 20.0 mag. At this level of brightness, only objects with redshift less than 0.5 can be observed, plus a few luminous high-redshift quasars, using this system. In order to test how well the system performs in the study of the structure of the local universe, we repeat the simulation with a redshift range

TABLE 4
DISPERSION COMPARISON OF $z_{\mathrm{STEP}} = 0.05$ AND 0.005

		σ_z		l		$\overline{\Delta z}$	
Δm	z_{step}	BATC	*UBVRI*	BATC	*UBVRI*	BATC	*UBVRI*
0.03	0.05	0.013	0.040	0.00	0.10	0.005	0.016
	0.005	0.006	0.039	0.00	0.00	0.000	0.014
0.05	0.05	0.016	0.055	0.00	1.00	0.005	0.024
	0.005	0.012	0.055	0.00	0.70	0.001	0.021
0.10	0.05	0.029	0.079	0.20	3.30	0.008	0.033
	0.005	0.028	0.081	0.00	3.40	0.005	0.029
0.20	0.05	0.062	0.103	2.30	9.50	0.016	0.042
	0.005	0.062	0.106	1.30	9.60	0.012	0.037
0.30	0.05	0.086	0.116	4.20	12.9	0.017	0.040
	0.005	0.086	0.120	4.10	13.0	0.012	0.034

NOTE.—Redshift range from $z = 0$ to 0.5.

of $z = 0$–0.5. The z_{step} is refined to 0.005 in order to carry out better differentiation. The results with z_{step} of 0.05 are given in Table 4, and the plot of z_{cat} versus z_{phot} is shown in Figure 3.

From Table 4 we see that, for the BATC system, the σ_z improves when z_{step} drops from 0.05 to 0.005. However, the improvement gradually diminishes when the magnitude error becomes larger. For the *UBVRI* system, however, σ_z becomes larger with increased magnitude errors when z_{step} is refined to 0.005. As for $\overline{\Delta z}$, it improves by about the same amount for both systems when z_{step} becomes 0.005. This is partly due to the fact that the accuracy of z_{phot} for lower redshift objects is better than that for higher redshift ones (Bolzonella et al. 2000; Massarotti et al. 2001b). The refinement of z_{step} also allows more flexibility when performing the fitting.

From this test it is clear that, to estimate z_{phot} precisely, we should not only adopt smaller z_{step} for fitting but also process the photometry as accurately as possible. From the comparison and analysis above, the BATC multicolor photometric system
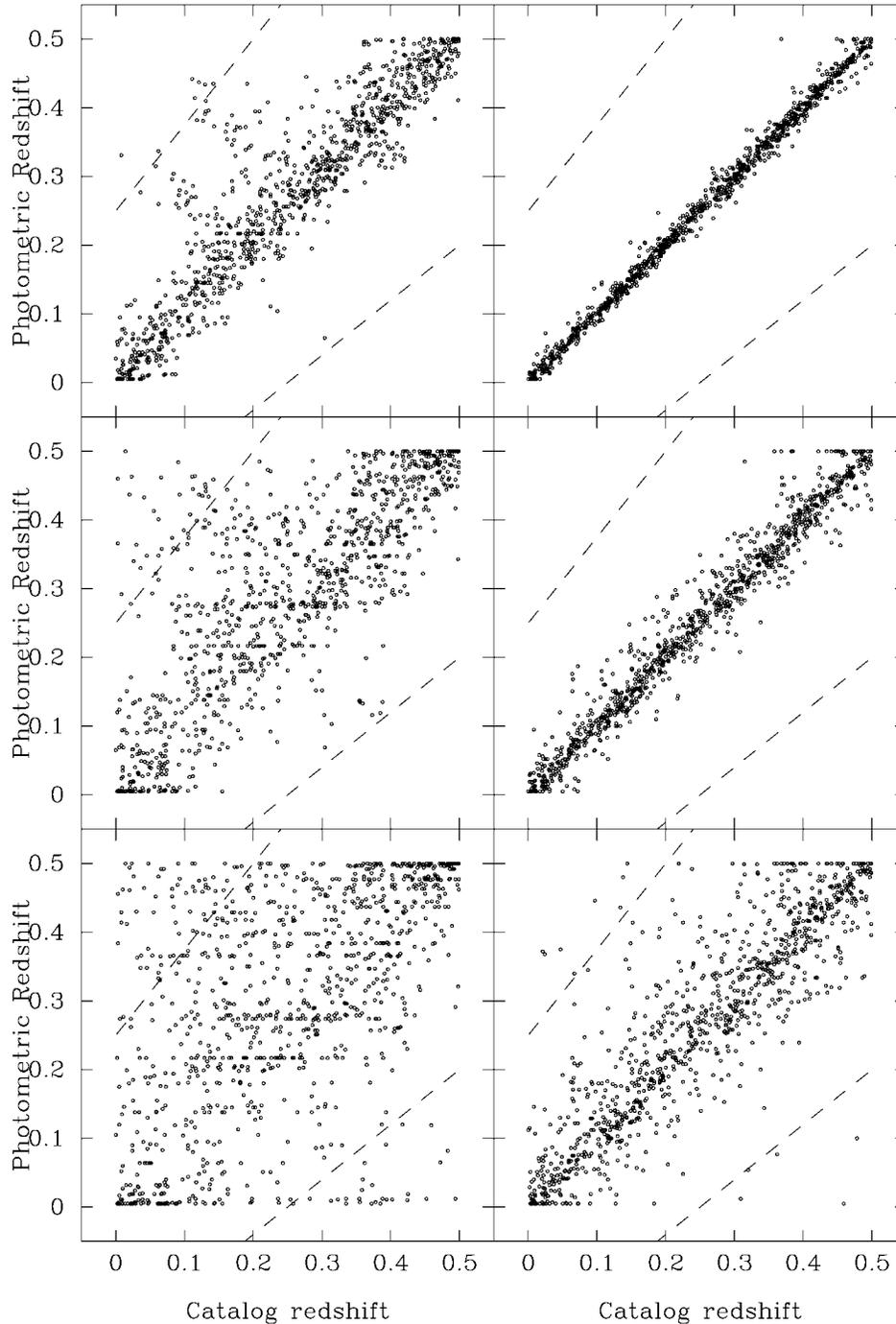
TABLE 3
SUMMARIZED RESULTS OF SOME OTHER AUTHORS

Source	Sample	Filters	Redshift Range	Δm	σ_z	$\overline{\Delta z}$
Bolzonella et al. 2000	Model	*UBVRI*	$z < 0.4$	0.05	0.07	0.03
				0.10	0.09	0.03
				0.20	0.20	0.11
				0.30	0.28	0.20
Fontana et al. 2000	Real	*UBVRIJK*	$z < 1.5$		0.08	
			$z > 2.0$		0.32	−0.144
Massarotti et al. 2001a	Real	*UBVIJHK*	$z < 1.5$		0.070	−0.001
			$z > 2.0$		0.177	−0.156
Fernández-Soto et al. 2001	Real	*UBVIJHK*	$z < 1.5$		0.110	0.002
			$2.0 < z < 4.0$		0.285	0.06
Le Borgne & Rocca-Volmerange 2002	Real	*UBVI*	$z < 1.5$		0.318	−0.127
		UBVIJHK	$z < 1.5$		0.098	0.021
Wolf et al. 2001	Real	16 color			0.03	0
Hickson et al. 1994	Model	40 bands (simulation)	$z < 0.5$	S/N = 10	<0.02	
				S/N = 3	0.06	
			$0.5 < z < 1.0$	S/N = 10	<0.01	
				S/N = 3	0.03	

FIG. 3.—Plot of catalog redshifts vs. fitted redshifts (z_{cat} vs. z_{phot}). Same as Fig. 2 but with the z_{step} refined to be 0.005. The fitted redshift range is from 0 to 0.5.

reveals its distinct advantage on z_{phot} estimation, especially for low-redshift objects. The typical value of σ_z can be as low as 0.02–0.03.

It should be pointed out that since the simulated catalog is created from templates, there exists the problem of incompleteness. Because all the tests are performed using these tem-

plates, when it comes to the analysis of real observations, certain spectra will not find their counterparts in the catalog, which consequently degrades the overall fitting quality.

The data in Tables 2 and 4 also indicate that, in a redshift range from 0 to 0.5, the systematic errors are all positive, which means that in this range the redshifts tend to be overestimated.

TABLE 5
ESTIMATED RESULTS USING SELECTED FILTER SETS

Number of Filters	Filters Used	σ_z	l	$\overline{\Delta z}$
15	a–p	0.011	0.00	0.001
14	a–o	0.011	0.00	0.001
13	a–n	0.012	0.00	0.001
12	a–m	0.012	0.00	0.001
11	a–k	0.013	0.00	0.001
10	a–j	0.013	0.00	0.001
9	a–i	0.014	0.00	0.001
8	a–h	0.016	0.00	0.002
7	a–g	0.018	0.40	0.002

On the other hand, for z from 0 to 6, the systematic errors are all negative, which means that the redshifts are being underestimated. This result agrees with the findings by Massarotti et al. (2001b).

5.2. Optimization of Redshift Survey from Filter Sets

The Balmer jump is the dominant spectral feature in wavelengths shorter than 6000 Å for galaxies with redshifts from 0 to 0.5. Below, we consider whether we could only use several crucial filters of shorter wavelengths to achieve the same goal, estimating z_{phot} properly, but at the same time maximize the observational efficiency. We perform this test by deleting longer wavelength filters, one at a time, from p to h (wavelength coverage decreases from 10000 to 6000 Å). The photometric error is chosen to be the typical value $\Delta m = 0.05$ mag. The redshift range is set from $z = 0$ to 0.5 with $z_{\mathrm{step}} = 0.005$. The results are summarized in Table 5.

In Table 5, column (1) lists the number of filters that are used when performing the estimation. Column (2) lists the corresponding labels of filters used; σ_z and l are defined as in Table 4. The first row in this table is the result using all 15 filters. No obvious degradation is seen until in the last case, which indicates that we can obtain accurate z_{phot} estimation for

TABLE 7
PHOTOMETRIC AND SPECTROSCOPIC REDSHIFTS OF GALAXIES
IN THE BATC T329 FIELD

No.	α (J2000.0)	δ (J2000.0)	z_{spec}	PSF PHOTOMETRY		APERTURE PHOTOMETRY	
				z_{phot}	Δz	z_{phot}	Δz
1	09 54 38.24	47 10 26.2	0.251	0.228	0.023	0.237	0.014
2	09 54 39.00	47 15 48.4	0.400	0.371	0.029	0.360	0.040
3	09 55 03.45	47 28 34.3	0.329	0.318	0.011	0.326	0.003
4	09 55 06.08	47 29 05.2	0.334	0.336	−0.002	0.479	−0.145
5	09 55 08.56	47 29 43.3	0.333	0.325	0.008	0.323	0.010
6	09 55 04.20	47 29 50.4	0.385	0.398	−0.013	0.311	0.074
7	09 55 08.96	47 29 54.0	0.332	0.329	0.003	0.330	0.002
8	09 55 12.78	47 30 32.1	0.335	0.387	−0.052	0.415	−0.080
9	09 54 03.77	47 40 04.5	0.247	0.259	−0.012	0.273	−0.026
10	09 54 05.22	47 41 32.5	0.250	0.229	0.021	0.237	0.013
11	09 54 00.67	47 58 05.1	0.537	0.520	0.017	0.518	0.019
12	09 54 24.46	47 58 41.1	0.307	0.335	−0.028	0.346	−0.039
13	09 54 26.93	47 58 53.9	0.296	0.300	−0.004	0.279	0.017
14	09 54 28.62	47 58 57.3	0.317	0.311	0.006	0.231	0.086
15	09 54 24.43	47 58 58.9	0.297	0.322	−0.025	0.350	−0.053
16	09 54 30.62	48 00 21.0	0.373	0.362	0.011	0.339	0.034
17	09 53 51.81	47 55 56.1	0.087	0.085	0.002	0.084	0.003

NOTE.—Units of right ascension are hours, minutes, and seconds, and units of declination are degrees, arcminutes, and arcseconds. For PSF photometry, $\overline{\Delta z} = 0.000$ and $\sigma_z = 0.021$. For aperture photometry, $\overline{\Delta z} = -0.002$ and $\sigma_z = 0.055$.

low-redshift objects using the BATC system with only eight filters, from a to h.

6. COMPARISON BETWEEN PHOTOMETRIC AND SPECTROSCOPIC REDSHIFTS

We have generated a set of 15 color SEDs for 27 galaxies with known z_{spec}, which can be used to check the accuracy of z_{phot} obtained with the BATC system.

We first estimate the z_{phot} for the 10 central member galaxies of Abell 566. Since these galaxies are the brightest in the cluster,

TABLE 6
FITTING RESULTS OF BATC TA03 FIELD (ABELL 566)

No.	α (J2000.0)	δ (J2000.0)	z_{spec}	$z_{\mathrm{step}} = 0.05$		$z_{\mathrm{step}} = 0.005$	
				z_{phot}	Δz	z_{phot}	Δz
1	07 04 43.12	63 18 38.9	0.09829	0.0950	0.003	0.0860	0.012
2	07 06 04.05	63 12 39.5	0.07884	0.0900	−0.011	0.0870	−0.008
3	07 04 07.90	63 08 06.7	0.09725	0.1000	−0.003	0.1020	−0.005
4	07 04 28.86	63 18 38.0	0.09479	0.0950	0.000	0.0910	0.004
5	07 04 39.85	63 19 18.3	0.09881	0.1000	−0.001	0.0980	0.001
6	07 05 33.97	63 15 26.4	0.10007	0.1050	−0.005	0.1030	−0.003
7	07 06 17.92	63 06 50.1	0.07910	0.1050	−0.026	0.0760	0.003
8	07 03 29.96	63 15 16.7	0.09969	0.1100	−0.010	0.1140	−0.014
9	07 03 46.65	63 19 27.0	0.09463	0.1050	−0.010	0.1030	−0.008
10	07 05 33.88	63 05 24.2	0.09319	0.0950	−0.002	0.0960	−0.003

NOTE.—Units of right ascension are hours, minutes, and seconds, and units of declination are degrees, arcminutes, and arcseconds. For $z_{\mathrm{step}} = 0.05$, $\overline{\Delta z} = -0.007$ and $\sigma_z = 0.008$. For $z_{\mathrm{step}} = 0.005$, $\overline{\Delta z} = -0.002$ and $\sigma_z = 0.008$.
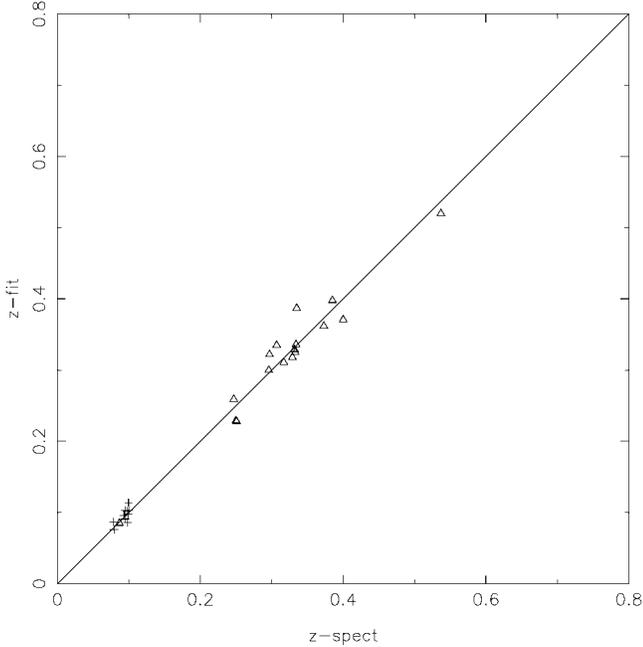
FIG. 4.—Plot of spectroscopic redshifts vs. fitted redshifts (z_{spec} vs. z_{phot}) of the galaxies in the TA03 and T329 fields. Triangles mark sources in the T329 field, and crosses represent sources in the TA01 field; z_{phot} of the TA03 field are obtained using aperture photometry, and those of the T329 field are obtained using PSF photometry.

their SEDs can be obtained with small photometric uncertainties. We adopt a value of 0.05 mag for the photometric uncertainty, which includes errors from observation and from subsequent flux calibration. By applying *hyperz* to the spectra with parameters of $z = 0$–0.5, $z_{\mathrm{step}} = 0.05$, $Av = 0$–0.3, and $Av_{\mathrm{step}} = 0.03$, z_{phot} for the 10 galaxies are obtained. The results are listed in Table 6. Here the range of Av is inferred from the best fit. We then refine the redshift step to $z_{\mathrm{step}} = 0.005$. The results with the refined step are given in columns (7) and (8) in Table 6. The accuracy remains about the same for the two choices of z_{step}. However, the systematic error is apparently improved from $\overline{\Delta z} = -0.007$ to -0.002. We thus confirm that our estimation can be improved by using smaller fitting steps and that the determination of photometric redshift can reach a higher precision for bright galaxies with smaller photometric errors.

Second, we also obtain the z_{phot} for the galaxies in the T329 field using aperture and PSF photometry, respectively. The parameters used are the same as above except for the photometric errors. For all 17 galaxies, the dispersion of the measurements σ_z is 0.021 for PSF photometry and 0.055 for aperture photometry. For the majority of these galaxies, the photometric redshifts are almost the same. For the other several galaxies, the relatively large deviations of z_{phot} are due to the differences in SED shapes. In addition, we examined the images carefully and found that the majority of sources with relatively

large deviations using aperture photometry are objects with other objects nearby. Therefore, it is apparent that PSF fitting is superior to the method of aperture photometry, especially when dealing with crowded fields. The comparison of z_{spec} to z_{phot} derived using two different methods is shown in Table 7, and z_{spec} versus z_{phot} are plotted for both galaxies in the TA03 and T329 fields in Figure 4; z_{phot} of the TA03 field are obtained using aperture photometry, and those of the T329 field are obtained using PSF photometry.

7. SUMMARY

In this paper, with the help of *hyperz*, we examine the accuracy of redshift estimation by comparing the BATC 15 intermediate-band photometric system to the *UBVRI* broadband photometric system using simulated spectra. We find that with the BATC system we can obtain fairly accurate redshift estimation. This advantage comes from the careful selection of the 15 color filter set in the beginning of the BATC survey. The z_{phot} determination of the spectroscopic sample in the BATC fields is also checked. The main results are as follows:

1. The uncertainty in photometric redshifts comes mainly from the photometric errors. We have made assessment of the accuracy with simulation. The dispersion can reach as low as $\sigma_z = 0.02$–0.03 with almost no catastrophic dropout for the typical photometric uncertainty from $\Delta m = 0.05$ to $\Delta m = 0.1$ mag.

2. The objects that can be observed with BATC survey are generally limited to a redshift range of 0–0.5, hence the filters whose central wavelengths are shorter than 6000 Å are especially important for the detection of the 4000 Å Balmer break. It has further been shown that we can use only the filters blueward of 6000 Å for the accurate determination of redshift and save significant amount of telescope time.

3. For the 10 brightest galaxies centered in Abell 566, the results show that the accuracy of photometric redshift determination is $\sigma_z = 0.008$ for z_{step} of 0.05 and 0.005, with systematic errors of $\overline{\Delta z} = -0.007$ and -0.002, respectively. For the 17 galaxies that have spectroscopic measurements in NED, the accuracy is $\sigma_z = 0.021$.

REFERENCES

Allen, C. W. 1976, Astrophysical Quantities (London: Athlone), 264

Bolzonella, M., Miralles, J.-M., & Pelló, R. 2000, A&A, 363, 476

Bruzual, A. G., & Charlot, S. 1993, ApJ, 405, 538

Coleman, G. D., Wu, C.-C., & Weedman, D. W. 1980, ApJS, 43, 393

Connolly, A. J., Csabai, I., Szalay, A. S., Koo, D. C., Kron, R. G., & Munn, J. A. 1995, AJ, 110, 2655

Corbin, M. R., Vacca, W. D., O'Neil, E., Thompson, R. I., Rieke, M. J., & Schneider, G. 2000, AJ, 119, 1062

Fan, X., et al. 1996, AJ, 112, 628

Fernández-Soto, A., Lanzetta, K. M., Chen, H-W., Pascarelle, S. M., & Yahata, N. 2001, ApJS, 135, 41

Fontana, A., D'Odorico, S., Poli, F., Giallongo, E., Arnouts, S., Cristiani, S., Moorwood, A., & Saracco, P. 2000, AJ, 120, 2206

Fukugita, M., Ichikawa, T., Gunn, J. E., Doi, M., Shimasaku, K., & Schneider, D. P. 1996, AJ, 111, 1748

Gal, R. R., de Carvalho, R. R., Brunner, R., Odewahn, S. C., & Djorgovski, S. G. 2000, AJ, 120, 540

Hickson, P., Gibson, B. K., & Callaghan, K. A. S. 1994, MNRAS, 267, 911

Holden, B. P., Nichol, R. C., Romer, A. K., Metevier, A., Postman, M., Ulmer, M. P., & Lubin, L. M. 1999, AJ, 118, 2002

Jenkner, H., Lasker, B. M., Sturch, C. R., McLean, B. J., Shara, M. M., & Russel, J. L. 1990, AJ, 99, 2082

Le Borgne, D., & Rocca-Volmerange, B. 2002, A&A, 386, 446

Massarotti, M., Iovino, A., & Buzzoni, A. 2001a, A&A, 368, 74

Massarotti, M., Iovino, A., Buzzoni, A., & Valls-Gabaud, D. 2001b, A&A, 380, 425

Oke, J. B., & Gunn, J. E. 1983, ApJ, 266, 713

Pascarelle, S. M., Lanzetta, K. M., & Fernández-Soto, A. 1998, ApJ, 508, L1

Postman, M., Lubin, L. M., Gunn, J. E. Oke, J. B., Hoessel, J. G., Schneider, D. P., & Christensen, J. A. 1996, AJ, 111, 615

Slinglend, K., Batuski, D., Miller, C., Haase, S., Michaud, K., & Hill, J. M. 1998, ApJS, 115, 1

Sowards-Emmerd, D., McKay, T. A., Sheldon, E., & Smith, J. A. 1999, AAS, 194, 0410

Stetson, P. B. 1987, PASP, 99, 191

Volonteri, M., Saracco, P., Chincarini, G., & Bolzonella, M. 2000, A&A, 362, 487

Wang, Y., Bahcall, N., & Turner, E. L. 1998, AJ, 116, 2081

Wolf, C., et al. 2001, A&A, 365, 681

Yahata, N., Lanzetta, K. M., Chen, H-W., Fernández-Soto, A., Pascarelle, S. M., Yahil, A., & Puetter, R. C. 2000, ApJ, 538, 493

Yan, H. J., et al. 2000, PASP, 112, 691

Yuan, Q., Zhou, X., Chen, J., Jiang, Z., Ma, J., Wu, H., Xue, S., & Zhu, J. 2001, AJ, 122, 1718

Zhou, X., Jiang, Z. J., Xue, S. J., Wu, H., Ma, J., & Chen, J. S. 2001, Chinese J. Astron. Astrophys., 1, 372

Zhou, X., et al. 2002, A&A, in press